

**J/ψ Production vs Centrality, Transverse Momentum, and Rapidity
in Au+Au collisions at $\sqrt{s_{NN}} = 200$ GeV**

A. Adare,⁸ S. Afanasiev,²² C. Aidala,⁹ N.N. Ajitanand,⁴⁹ Y. Akiba,^{43,44} H. Al-Bataineh,³⁸ J. Alexander,⁴⁹
A. Al-Jamel,³⁸ K. Aoki,^{28,43} L. Aphecetche,⁵¹ R. Armendariz,³⁸ S.H. Aronson,³ J. Asai,⁴⁴ E.T. Atomssa,²⁹
R. Averbeck,⁵⁰ T.C. Awes,³⁹ B. Azmoun,³ V. Babintsev,¹⁸ G. Baksay,¹⁴ L. Baksay,¹⁴ A. Baldissieri,¹¹ K.N. Barish,⁴
P.D. Barnes,³¹ B. Bassalleck,³⁷ S. Bathe,⁴ S. Batsouli,^{9,39} V. Baublis,⁴² F. Bauer,⁴ A. Bazilevsky,³ S. Belikov,^{3,21}
R. Bennett,⁵⁰ Y. Berdnikov,⁴⁶ A.A. Bickley,⁸ M.T. Bjorndal,⁹ J.G. Boissevain,³¹ H. Borel,¹¹ K. Boyle,⁵⁰
M.L. Brooks,³¹ D.S. Brown,³⁸ D. Bucher,³⁴ H. Buesching,³ V. Bumazhnov,¹⁸ G. Bunce,^{3,44} J.M. Burward-Hoy,³¹
S. Butsyk,^{31,50} S. Campbell,⁵⁰ J.-S. Chai,²³ B.S. Chang,⁵⁸ J.-L. Charvet,¹¹ S. Chernichenko,¹⁸ J. Chiba,²⁴
C.Y. Chi,⁹ M. Chiu,^{9,19} I.J. Choi,⁵⁸ T. Chujo,⁵⁵ P. Chung,⁴⁹ A. Churnin,¹⁸ V. Cianciolo,³⁹ C.R. Clevin,¹⁶
Y. Cobigo,¹¹ B.A. Cole,⁹ M.P. Comets,⁴⁰ P. Constantin,^{21,31} M. Csanád,¹³ T. Csörgő,²⁵ T. Dahms,⁵⁰ K. Das,¹⁵
G. David,³ M.B. Deaton,¹ K. Dehmelt,¹⁴ H. Delagrange,⁵¹ A. Denisov,¹⁸ D. d'Enterria,⁹ A. Deshpande,^{44,50}
E.J. Desmond,³ O. Dietzsch,⁴⁷ A. Dion,⁵⁰ M. Donadelli,⁴⁷ J.L. Drachenberg,¹ O. Drapier,²⁹ A. Drees,⁵⁰
A.K. Dubey,⁵⁷ A. Durum,¹⁸ V. Dzhordzhadze,^{4,52} Y.V. Efremenko,³⁹ J. Egdemir,⁵⁰ F. Ellinghaus,⁸ W.S. Emam,⁴
A. Enokizono,^{17,30} H. En'yo,^{43,44} B. Espagnon,⁴⁰ S. Esumi,⁵⁴ K.O. Eyster,⁴ D.E. Fields,^{37,44} M. Finger,^{5,22}
F. Fleuret,²⁹ S.L. Fokin,²⁷ B. Forestier,³² Z. Fraenkel,⁵⁷ J.E. Frantz,^{9,50} A. Franz,³ A.D. Frawley,¹⁵ K. Fujiwara,⁴³
Y. Fukao,^{28,43} S.-Y. Fung,⁴ T. Fusayasu,³⁶ S. Gadrat,³² I. Garishvili,⁵² F. Gastineau,⁵¹ M. Germain,⁵¹ A. Glenn,^{8,52}
H. Gong,⁵⁰ M. Gonin,²⁹ J. Gosset,¹¹ Y. Goto,^{43,44} R. Granier de Cassagnac,²⁹ N. Grau,²¹ S.V. Greene,⁵⁵
M. Grosse Perdekamp,^{19,44} T. Gunji,⁷ H.-Å. Gustafsson,³³ T. Hachiya,^{17,43} A. Hadj Henni,⁵¹ C. Haegemann,³⁷
J.S. Haggerty,³ M.N. Hagiwara,¹ H. Hamagaki,⁷ R. Han,⁴¹ H. Harada,¹⁷ E.P. Hartouni,³⁰ K. Haruna,¹⁷ M. Harvey,³
E. Haslum,³³ K. Hasuko,⁴³ R. Hayano,⁷ M. Heffner,³⁰ T.K. Hemmick,⁵⁰ T. Hester,⁴ J.M. Heuser,⁴³ X. He,¹⁶
H. Hiejima,¹⁹ J.C. Hill,²¹ R. Hobbs,³⁷ M. Hohlmann,¹⁴ M. Holmes,⁵⁵ W. Holzmann,⁴⁹ K. Homma,¹⁷ B. Hong,²⁶
T. Horaguchi,^{43,53} D. Hornback,⁵² M.G. Hur,²³ T. Ichihara,^{43,44} K. Imai,^{28,43} M. Inaba,⁵⁴ Y. Inoue,^{45,43}
D. Isenhower,¹ L. Isenhower,¹ M. Ishihara,⁴³ T. Isobe,⁷ M. Issah,⁴⁹ A. Isupov,²² B.V. Jacak,⁵⁰ J. Jia,⁹ J. Jin,⁹
O. Jinnouchi,⁴⁴ B.M. Johnson,³ K.S. Joo,³⁵ D. Jouan,⁴⁰ F. Kajihara,^{7,43} S. Kametani,^{7,56} N. Kamihara,^{43,53}
J. Kamin,⁵⁰ M. Kaneta,⁴⁴ J.H. Kang,⁵⁸ H. Kanou,^{43,53} T. Kawagishi,⁵⁴ D. Kawall,⁴⁴ A.V. Kazantsev,²⁷
S. Kelly,⁸ A. Khanzadeev,⁴² J. Kikuchi,⁵⁶ D.H. Kim,³⁵ D.J. Kim,⁵⁸ E. Kim,⁴⁸ Y.-S. Kim,²³ E. Kinney,⁸
A. Kiss,¹³ E. Kistenev,³ A. Kiyomichi,⁴³ J. Klay,³⁰ C. Klein-Boesing,³⁴ L. Kochenda,⁴² V. Kochetkov,¹⁸
B. Komkov,⁴² M. Konno,⁵⁴ D. Kotchetkov,⁴ A. Kozlov,⁵⁷ A. Král,¹⁰ A. Kravitz,⁹ P.J. Kroon,³ J. Kubart,^{5,20}
G.J. Kunde,³¹ N. Kurihara,⁷ K. Kurita,^{45,43} M.J. Kweon,²⁶ Y. Kwon,^{52,58} G.S. Kyle,³⁸ R. Lacey,⁴⁹ Y.-S. Lai,⁹
J.G. Lajoie,²¹ A. Lebedev,²¹ Y. Le Bornec,⁴⁰ S. Leckey,⁵⁰ D.M. Lee,³¹ M.K. Lee,⁵⁸ T. Lee,⁴⁸ M.J. Leitch,³¹
M.A.L. Leite,⁴⁷ B. Lenzi,⁴⁷ H. Lim,⁴⁸ T. Liška,¹⁰ A. Litvinenko,²² M.X. Liu,³¹ X. Li,⁶ X.H. Li,⁴ B. Love,⁵⁵
D. Lynch,³ C.F. Maguire,⁵⁵ Y.I. Makdisi,³ A. Malakhov,²² M.D. Malik,³⁷ V.I. Manko,²⁷ Y. Mao,^{41,43} L. Mašek,^{5,20}
H. Masui,⁵⁴ F. Matathias,^{9,50} M.C. McCain,¹⁹ M. McCumber,⁵⁰ P.L. McGaughey,³¹ Y. Miake,⁵⁴ P. Mikeš,^{5,20}
K. Miki,⁵⁴ T.E. Miller,⁵⁵ A. Milov,⁵⁰ S. Mioduszewski,³ G.C. Mishra,¹⁶ M. Mishra,² J.T. Mitchell,³ M. Mitrovski,⁴⁹
A. Morreale,⁴ D.P. Morrison,³ J.M. Moss,³¹ T.V. Moukhanova,²⁷ D. Mukhopadhyay,⁵⁵ J. Murata,^{45,43}
S. Nagamiya,²⁴ Y. Nagata,⁵⁴ J.L. Nagle,⁸ M. Naglis,⁵⁷ I. Nakagawa,^{43,44} Y. Nakamiya,¹⁷ T. Nakamura,¹⁷
K. Nakano,^{43,53} J. Newby,³⁰ M. Nguyen,⁵⁰ B.E. Norman,³¹ A.S. Nyanin,²⁷ J. Nystrand,³³ E. O'Brien,³ S.X. Oda,⁷
C.A. Ogilvie,²¹ H. Ohnishi,⁴³ I.D. Ojha,⁵⁵ H. Okada,^{28,43} K. Okada,⁴⁴ M. Oka,⁵⁴ O.O. Omiwade,¹ A. Oskarsson,³³
I. Otterlund,³³ M. Ouchida,¹⁷ K. Ozawa,⁷ R. Pak,³ D. Pal,⁵⁵ A.P.T. Palounek,³¹ V. Pantuev,⁵⁰ V. Papavassiliou,³⁸
J. Park,⁴⁸ W.J. Park,²⁶ S.F. Pate,³⁸ H. Pei,²¹ J.-C. Peng,¹⁹ H. Pereira,¹¹ V. Peresedov,²² D.Yu. Peressounko,²⁷
C. Pinkenburg,³ R.P. Pisani,³ M.L. Purschke,³ A.K. Purwar,^{31,50} H. Qu,¹⁶ J. Rak,^{21,37} A. Rakotozafindrabe,²⁹
I. Ravinovich,⁵⁷ K.F. Read,^{39,52} S. Rembeczki,¹⁴ M. Reuter,⁵⁰ K. Reygers,³⁴ V. Riabov,⁴² Y. Riabov,⁴²
G. Roche,³² A. Romana,^{29,*} M. Rosati,²¹ S.S.E. Rosendahl,³³ P. Rosnet,³² P. Rukoyatkin,²² V.L. Rykov,⁴³
S.S. Ryu,⁵⁸ B. Sahlmueller,³⁴ N. Saito,^{28,43,44} T. Sakaguchi,^{3,7,56} S. Sakai,⁵⁴ H. Sakata,¹⁷ V. Samsonov,⁴²
H.D. Sato,^{28,43} S. Sato,^{3,24,54} S. Sawada,²⁴ J. Seele,⁸ R. Seidl,¹⁹ V. Semenov,¹⁸ R. Seto,⁴ D. Sharma,⁵⁷ T.K. Shea,³
I. Shein,¹⁸ A. Shevel,^{42,49} T.-A. Shibata,^{43,53} K. Shigaki,¹⁷ M. Shimomura,⁵⁴ T. Shohjoh,⁵⁴ K. Shoji,^{28,43}
A. Sickles,⁵⁰ C.L. Silva,⁴⁷ D. Silvermyr,³⁹ C. Silvestre,¹¹ K.S. Sim,²⁶ C.P. Singh,² V. Singh,² S. Skutnik,²¹
M. Slunečka,^{5,22} W.C. Smith,¹ A. Soldatov,¹⁸ R.A. Soltz,³⁰ W.E. Sondheim,³¹ S.P. Sorensen,⁵² I.V. Sourikova,³
F. Staley,¹¹ P.W. Stankus,³⁹ E. Stenlund,³³ M. Stepanov,³⁸ A. Ster,²⁵ S.P. Stoll,³ T. Sugitate,¹⁷ C. Suire,⁴⁰

J.P. Sullivan,³¹ J. Sziklai,²⁵ T. Tabaru,⁴⁴ S. Takagi,⁵⁴ E.M. Takagui,⁴⁷ A. Taketani,^{43,44} K.H. Tanaka,²⁴ Y. Tanaka,³⁶ K. Tanida,^{43,44} M.J. Tannenbaum,³ A. Taranenko,⁴⁹ P. Tarján,¹² T.L. Thomas,³⁷ M. Togawa,^{28,43} A. Toia,⁵⁰ J. Tojo,⁴³ L. Tomášek,²⁰ H. Torii,⁴³ R.S. Towell,¹ V-N. Tram,²⁹ I. Tserruya,⁵⁷ Y. Tsuchimoto,^{17,43} S.K. Tuli,² H. Tydesjö,³³ N. Tyurin,¹⁸ C. Vale,²¹ H. Valle,⁵⁵ H.W. van Hecke,³¹ J. Velkovska,⁵⁵ R. Vertesi,¹² A.A. Vinogradov,²⁷ M. Virius,¹⁰ V. Vrba,²⁰ E. Vznuzdaev,⁴² M. Wagner,^{28,43} D. Walker,⁵⁰ X.R. Wang,³⁸ Y. Watanabe,^{43,44} J. Wessels,³⁴ S.N. White,³ N. Willis,⁴⁰ D. Winter,⁹ C.L. Woody,³ M. Wysocki,⁸ W. Xie,^{4,44} Y. Yamaguchi,⁵⁶ A. Yanovich,¹⁸ Z. Yasin,⁴ J. Ying,¹⁶ S. Yokkaichi,^{43,44} G.R. Young,³⁹ I. Younus,³⁷ I.E. Yushmanov,²⁷ W.A. Zajc,^{9,†} O. Zaudtke,³⁴ C. Zhang,^{9,39} S. Zhou,⁶ J. Zimányi,^{25,*} and L. Zolin²²

(PHENIX Collaboration)

¹Abilene Christian University, Abilene, TX 79699, U.S.

²Department of Physics, Banaras Hindu University, Varanasi 221005, India

³Brookhaven National Laboratory, Upton, NY 11973-5000, U.S.

⁴University of California - Riverside, Riverside, CA 92521, U.S.

⁵Charles University, Ovocný trh 5, Praha 1, 116 36, Prague, Czech Republic

⁶China Institute of Atomic Energy (CIAE), Beijing, People's Republic of China

⁷Center for Nuclear Study, Graduate School of Science, University of Tokyo, 7-3-1 Hongo, Bunkyo, Tokyo 113-0033, Japan

⁸University of Colorado, Boulder, CO 80309, U.S.

⁹Columbia University, New York, NY 10027 and Nevis Laboratories, Irvington, NY 10533, U.S.

¹⁰Czech Technical University, Zikova 4, 166 36 Prague 6, Czech Republic

¹¹Dapnia, CEA Saclay, F-91191, Gif-sur-Yvette, France

¹²Debrecen University, H-4010 Debrecen, Egyetem tér 1, Hungary

¹³ELTE, Eötvös Loránd University, H - 1117 Budapest, Pázmány P. s. 1/A, Hungary

¹⁴Florida Institute of Technology, Melbourne, FL 32901, U.S.

¹⁵Florida State University, Tallahassee, FL 32306, U.S.

¹⁶Georgia State University, Atlanta, GA 30303, U.S.

¹⁷Hiroshima University, Kagamiyama, Higashi-Hiroshima 739-8526, Japan

¹⁸IHEP Protvino, State Research Center of Russian Federation, Institute for High Energy Physics, Protvino, 142281, Russia

¹⁹University of Illinois at Urbana-Champaign, Urbana, IL 61801, U.S.

²⁰Institute of Physics, Academy of Sciences of the Czech Republic, Na Slovance 2, 182 21 Prague 8, Czech Republic

²¹Iowa State University, Ames, IA 50011, U.S.

²²Joint Institute for Nuclear Research, 141980 Dubna, Moscow Region, Russia

²³KAERI, Cyclotron Application Laboratory, Seoul, South Korea

²⁴KEK, High Energy Accelerator Research Organization, Tsukuba, Ibaraki 305-0801, Japan

²⁵KFKI Research Institute for Particle and Nuclear Physics of the Hungarian Academy of Sciences (MTA KFKI RMKI), H-1525 Budapest 114, POBox 49, Budapest, Hungary

²⁶Korea University, Seoul, 136-701, Korea

²⁷Russian Research Center "Kurchatov Institute", Moscow, Russia

²⁸Kyoto University, Kyoto 606-8502, Japan

²⁹Laboratoire Leprince-Ringuet, Ecole Polytechnique, CNRS-IN2P3, Route de Saclay, F-91128, Palaiseau, France

³⁰Lawrence Livermore National Laboratory, Livermore, CA 94550, U.S.

³¹Los Alamos National Laboratory, Los Alamos, NM 87545, U.S.

³²LPC, Université Blaise Pascal, CNRS-IN2P3, Clermont-Fd, 63177 Aubiere Cedex, France

³³Department of Physics, Lund University, Box 118, SE-221 00 Lund, Sweden

³⁴Institut für Kernphysik, University of Muenster, D-48149 Muenster, Germany

³⁵Myongji University, Yongin, Kyonggido 449-728, Korea

³⁶Nagasaki Institute of Applied Science, Nagasaki-shi, Nagasaki 851-0193, Japan

³⁷University of New Mexico, Albuquerque, NM 87131, U.S.

³⁸New Mexico State University, Las Cruces, NM 88003, U.S.

³⁹Oak Ridge National Laboratory, Oak Ridge, TN 37831, U.S.

⁴⁰IPN-Orsay, Université Paris Sud, CNRS-IN2P3, BP1, F-91406, Orsay, France

⁴¹Peking University, Beijing, People's Republic of China

⁴²PNPI, Petersburg Nuclear Physics Institute, Gatchina, Leningrad region, 188300, Russia

⁴³RIKEN, The Institute of Physical and Chemical Research, Wako, Saitama 351-0198, Japan

⁴⁴RIKEN BNL Research Center, Brookhaven National Laboratory, Upton, NY 11973-5000, U.S.

⁴⁵Physics Department, Rikkyo University, 3-34-1 Nishi-Ikebukuro, Toshima, Tokyo 171-8501, Japan

⁴⁶Saint Petersburg State Polytechnic University, St. Petersburg, Russia

⁴⁷Universidade de São Paulo, Instituto de Física, Caixa Postal 66318, São Paulo CEP05315-970, Brazil

⁴⁸System Electronics Laboratory, Seoul National University, Seoul, South Korea

⁴⁹Chemistry Department, Stony Brook University, Stony Brook, SUNY, NY 11794-3400, U.S.

⁵⁰Department of Physics and Astronomy, Stony Brook University, SUNY, Stony Brook, NY 11794, U.S.

⁵¹SUBATECH (Ecole des Mines de Nantes, CNRS-IN2P3, Université de Nantes) BP 20722 - 44307, Nantes, France

⁵²University of Tennessee, Knoxville, TN 37996, U.S.

⁵³Department of Physics, Tokyo Institute of Technology, Oh-okayama, Meguro, Tokyo 152-8551, Japan

⁵⁴Institute of Physics, University of Tsukuba, Tsukuba, Ibaraki 305, Japan

⁵⁵Vanderbilt University, Nashville, TN 37235, U.S.

⁵⁶Waseda University, Advanced Research Institute for Science and Engineering, 17 Kikui-cho, Shinjuku-ku, Tokyo 162-0044, Japan

⁵⁷Weizmann Institute, Rehovot 76100, Israel

⁵⁸Yonsei University, IPAP, Seoul 120-749, Korea

The PHENIX experiment at the Relativistic Heavy Ion Collider (RHIC) has measured J/ψ production for rapidities $-2.2 < y < 2.2$ in Au + Au collisions at $\sqrt{s_{NN}} = 200$ GeV. The J/ψ invariant yield and nuclear modification factor R_{AA} as a function of centrality, transverse momentum and rapidity are reported. A suppression of J/ψ relative to binary collision scaling of proton-proton reaction yields is observed. Models which describe the lower energy J/ψ data at the Super Proton Synchrotron (SPS) invoking only J/ψ destruction based on the local medium density would predict a significantly larger suppression at RHIC and more suppression at mid rapidity than at forward rapidity. Both trends are contradicted by our data.

PACS numbers: 25.75.Dw

The Quark-Gluon-Plasma (QGP) is a state of deconfined quarks and gluons which is predicted by lattice Quantum Chromodynamics (QCD) calculations to be formed above a temperature of order $T_c = 170$ MeV for a baryon chemical potential $\mu_b = 0$ [1]. Heavy quarkonia (J/ψ , ψ' , χ_c and Υ) have long been considered one of the most promising probes to study formation and properties of QGP. In the deconfined state, the attraction between heavy quarks and anti-quarks is predicted to be reduced due to dynamic screening effects, leading to the suppression of heavy quarkonia yield. The strength of the suppression depends on the binding energies of the quarkonia and the temperature of the surrounding system [2]. Recent lattice QCD calculations suggest that the J/ψ may not dissociate until well above T_c [3, 4]. On the other hand χ_c and ψ' which contribute to the total J/ψ yield via decay are expected to dissolve at lower temperatures due to smaller binding energies.

A J/ψ suppression observed at lower energies by the NA50 experiment at the SPS [5, 6] could be reproduced by various theoretical calculations, some invoking QGP formation and others not. A larger suppression is expected at RHIC compared to SPS due to the larger energy density of the medium created [7, 8]. On the other hand, several models predict that the J/ψ yield will result from a balance between destruction due to thermal gluons and enhancement due to coalescence of uncorrelated $c\bar{c}$ pairs [7, 9], which are produced abundantly in the initial collisions at RHIC energy [10, 11]. Cold nuclear matter (CNM) effects such as nuclear absorption, shadowing and anti-shadowing are also expected to modify the J/ψ yield. PHENIX $d + Au$ data show that CNM effects are smaller at RHIC than those observed at lower energy [12] and can be reproduced by a nuclear absorption cross-section of up to 3 mb plus nuclear shadowing [13].

We report results on J/ψ production measured by the PHENIX collaboration at mid-rapidity ($|y| < 0.35$) via

e^+e^- decay and at forward rapidity ($|y| \in [1.2, 2.2]$) via $\mu^+\mu^-$ decay in Au + Au collisions at $\sqrt{s_{NN}} = 200$ GeV. These results do not separate primordial J/ψ and J/ψ from χ_c , ψ' or B decay. The J/ψ invariant yields as a function of centrality, rapidity (y) and transverse momentum (p_T) are shown. They are combined with the J/ψ yield measured in $p + p$ collisions [14] to form the J/ψ nuclear modification factor R_{AA} .

The PHENIX apparatus is described in [15]. At mid-rapidity electrons are measured with two spectrometers consisting of Drift Chambers (DC), Pad Chambers (PC), Ring Imaging Cerenkov Counters (RICH), and Electromagnetic Calorimeters (EMCal). They are identified by matching charged tracks reconstructed with the DC and the first layer of the PC to clusters in the EMCal and to hits in the RICH. The energy-momentum matching requirement is $(E/p - 1) \geq -2.5$ standard deviations (σ). The position matching between the track and the cluster in the EMCal is $\leq 2.5\sigma$ (4σ) in azimuth and along the beam axis, for central (peripheral) collisions. For the RICH, at least 4 (2) matching hits are required. Muons are measured with two forward spectrometers consisting of a front absorber to stop most hadrons produced in the collision, cathode strip chambers (MuTr) which provide momentum information and a Muon Identifier (MuID) which uses alternating layers of steel absorber and Iarocci tubes. Charged particle trajectories are first reconstructed in the MuID then in the MuTr. They must reach the last plane of the MuID and have a good geometrical match between the MuID and the MuTr to be identified as muons. The matching is $< 9^\circ$ for the slope and < 15 (20) cm for the position in the first layer of the MuID at positive (negative) rapidity. The collision centrality is determined using two Beam-Beam Counters (BBC) and Zero Degree Calorimeters (ZDC) [16].

The data used for this analysis were collected during the 2004 run at RHIC using a minimum bias trigger (a coincidence of the two BBC) which covers $92 \pm 3\%$ of the

Au + Au inelastic cross-section. After quality assurance and vertex cut ($|z| \leq 30$ cm), 9.9×10^8 (1.1×10^9) events were analyzed for mid (forward) rapidity, corresponding to an integrated luminosity of $157 \mu\text{b}^{-1}$ ($174 \mu\text{b}^{-1}$). The forward rapidity data were filtered using an offline level-2 trigger which provides a fast reconstruction of the particle trajectory in the MuID. Events are accepted by this filter when at least two good quality tracks reaching the last plane of the MuID are found within the acceptance.

The J/ψ yield is obtained from the unlike sign dilepton invariant mass distribution after subtracting the combinatorial background using an event-mixing technique. The background is normalized to the real data using the like-sign dilepton invariant mass distribution, $2\sqrt{N^{++}N^{--}}$, with N^{++} (N^{--}) being the number of positive (negative) dilepton pairs. The accuracy of the normalization is estimated to be 2 % and accounted for in the systematic errors. At midrapidity the J/ψ mass resolution is ~ 35 MeV/ c^2 . The number of J/ψ is determined by counting the remaining unlike sign pairs in the mass range $2.9 \leq M_{e^+e^-} \leq 3.3$ GeV/ c^2 . This number is corrected by the estimated contribution of the dielectron continuum and the loss due to the radiative tail. A total of ~ 1000 J/ψ are obtained and the signal to background (S/B) varies from 0.5 for central collisions to 15 for peripheral collisions. At forward rapidity, the J/ψ mass resolution varies from 150 to 200 MeV/ c^2 and is larger than at midrapidity primarily because of the multiple scattering and energy loss straggling in the front absorber. The residual background (notably from the open charm pairs and Drell-Yan) in the unlike-sign invariant mass distribution is evaluated using an exponential form. The J/ψ signal is estimated with direct counting of the remaining pairs in the mass range $2.6 \leq M_{\mu^+\mu^-} \leq 3.6$ GeV/ c^2 and using a fit with different line shapes. The average of the resulting values is used as the number of J/ψ and their dispersion is included in the systematic error. A total of ~ 4500 J/ψ are obtained and S/B varies from 0.2 for central collisions to 3 for peripheral collisions.

The J/ψ invariant yield in a given centrality, p_T and y bin is:

$$\frac{B_{ll}}{2\pi p_T} \frac{d^2 N_{J/\psi}}{dp_T dy} = \frac{1}{2\pi p_T} \frac{N_{J/\psi}}{N_{evt} \Delta y \Delta p_T A \epsilon} \quad (1)$$

with B_{ll} being the branching ratio for $J/\psi \rightarrow l^+l^-$; $N_{J/\psi}$ the number of J/ψ measured in the centrality bin; N_{evt} the corresponding number of events; Δy the rapidity range; Δp_T the transverse momentum range and $A\epsilon$ the acceptance and efficiency correction for J/ψ . $A\epsilon$ is determined by full GEANT simulation. It decreases with the collision centrality due to overlapping hits in the RICH, EMCal and MuTr, leading to an increasing amount of mis-reconstructed tracks which are then rejected by the analysis cuts. This effect is evaluated by embedding simulated J/ψ in real events. For the most central collisions

TABLE I: Sources of systematic errors on the J/ψ invariant yield. Columns 2 (3) are the average values at mid (forward) rapidity. When two values are given, the first (second) is for peripheral (central) collisions. Errors of type A (type B) are point to point uncorrelated (correlated).

source	$ y < 0.35$	$ y \in [1.2, 2.2]$	type
signal extraction	6.5 to 9 %	4 to 24 %	A
acceptance	6 %	10 %	B
efficiency	4.5 to 8 %	4 to 16 %	B
run by run variation	4 %	5 %	B
input y , p_T distributions	2 %	4 %	B

the efficiency loss is 20 % at mid rapidity and 75 % (50 %) at positive (negative) rapidity.

The nuclear modification factor in a given centrality, p_T and y bin is:

$$R_{AA} = \frac{d^2 N_{J/\psi}^{AA}/dp_T dy}{N_{coll} d^2 N_{J/\psi}^{pp}/dp_T dy} \quad (2)$$

with $d^2 N_{J/\psi}^{AA}/dp_T dy$ being the J/ψ yield in Au + Au collisions in the centrality bin, N_{coll} the corresponding mean number of binary collisions and $d^2 N_{J/\psi}^{pp}/dp_T dy$ the J/ψ yield in $p + p$ inelastic collisions.

The systematic errors on the J/ψ invariant yield (Table I) are grouped into three categories: point to point uncorrelated (type A) for which the points can move independently one from the other; point to point correlated (type B) for which the points can move coherently though not necessarily by the same amount; and global errors for which all points move by the same relative amount. Statistical and uncorrelated systematic errors are summed in quadrature and represented with vertical bars; correlated systematic errors are represented with boxes and different colors/symbols are used for forward and mid rapidity because they are independent; global systematic errors are quoted directly on the figures. For R_{AA} , additional systematic errors are associated with uncertainties in the calculation of N_{coll} (10 to 28 %) and the J/ψ yield in $p + p$ (12 % and 7 % at mid and forward rapidity, respectively). On the other hand the systematic errors that are common to Au + Au and $p + p$ cancel.

Figure 1 shows the J/ψ yield vs. p_T for different centrality bins (see Table II for the corresponding number of participants, N_{part}). Data from the two muon spectrometers are combined to obtain the forward rapidity points. In each centrality bin, the J/ψ mean square transverse momentum, $\langle p_T^2 \rangle$, is numerically calculated from the data for $p_T \leq 5$ GeV/ c and is shown in Table II. The first error corresponds to the statistical and uncorrelated systematic error on the J/ψ yield. The second corresponds to the correlated systematic error. At midrapidity the $\langle p_T^2 \rangle$ shows no variation versus centrality within

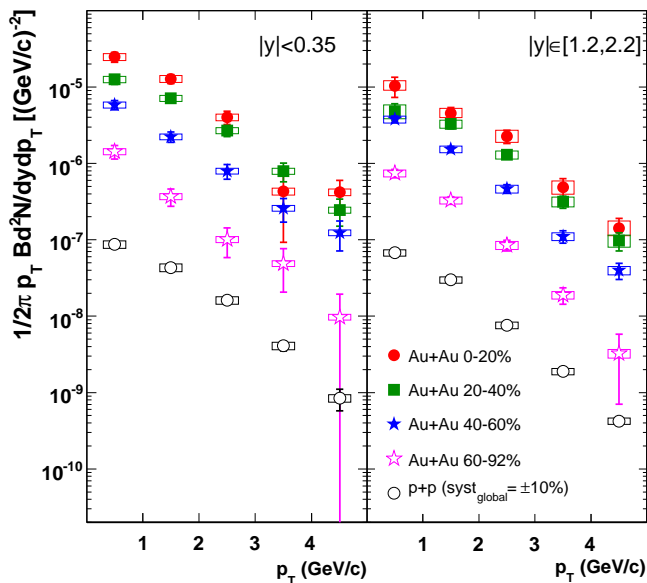


FIG. 1: J/ψ invariant yield vs. p_T for different centrality bins in Au + Au collisions and in $p + p$ collisions [14]. The left (right) panel corresponds to mid (forward) rapidity. See text for description of the errors.

TABLE II: Characterization of the J/ψ p_T and y distributions. Column 3 (4): J/ψ $\langle p_T^2 \rangle$ calculated for $p_T \leq 5$ GeV/c at mid (forward) rapidity for different centrality bins in Au + Au collisions and in $p + p$ collisions. The errors are described in the text. Column 5: Calculated RMS of the corresponding J/ψ y distributions.

cent (%)	N_{part}	$\langle p_T^2 \rangle$ (GeV/c) ²		y RMS
		$ y < 0.35$	$1.2 < y < 2.2$	
0-20	280	$3.6 \pm 0.6 \pm 0.1$	$4.4 \pm 0.4 \pm 0.4$	1.32 ± 0.06
20-40	140	$4.6 \pm 0.5 \pm 0.1$	$4.6 \pm 0.3 \pm 0.4$	1.30 ± 0.05
40-60	60	$4.5 \pm 0.7 \pm 0.2$	$3.7 \pm 0.2 \pm 0.3$	1.40 ± 0.04
60-92	14	$3.6 \pm 0.9 \pm 0.2$	$3.3 \pm 0.3 \pm 0.2$	1.43 ± 0.04
$p + p$	2	$4.1 \pm 0.2 \pm 0.1$	$3.4 \pm 0.1 \pm 0.1$	1.41 ± 0.03

the error bars. It increases slightly with N_{part} at forward rapidity.

Figure 2 shows the J/ψ yield (integrated over p_T) vs. y for different centrality bins. The root mean square (RMS) of each distribution is shown in Table II. For the two most peripheral bins (40-60 % and 60-93 %) the RMS is compatible with that measured in $p + p$ collisions. For the most central bins (0-20 % and 20-40 %), the RMS is smaller by about 2σ .

Figures 3 and 4 show the J/ψ R_{AA} vs. p_T and y , respectively, for different centrality bins. Figure 5(a) shows the p_T integrated R_{AA} vs. N_{part} at mid and forward rapidity. For each rapidity, R_{AA} decreases with increasing N_{part} . For the most central collisions, R_{AA} is below 0.3 (0.2) at mid (forward) rapidity. Figure 5(b) shows the

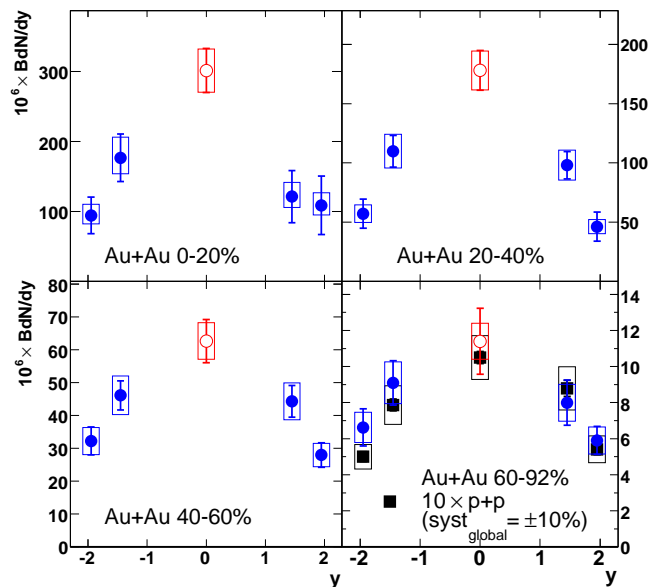


FIG. 2: J/ψ invariant yield vs. y for different centrality bins in Au + Au collisions and for $p + p$ collisions. Open (filled) circles are for mid (forward) rapidity Au + Au data. Black squares are for $p + p$ data [14]. See text for description of the errors.

ratio of forward/mid rapidity R_{AA} vs. N_{part} . The ratio first decreases then reaches a plateau of about 0.6 for $N_{\text{part}} > 100$.

We observed a significant J/ψ suppression relative to binary scaling of proton-proton is observed for central Au + Au collisions at RHIC. The magnitude of the suppression is similar to that observed at the SPS [6] and greater than the suppression expected by extrapolating the cold nuclear matter effects measured in $d + Au$ collisions [12, 13]. Models that describe the SPS data using a J/ψ and/or χ_c and ψ' suppression based on the local density predict a significantly larger suppression at RHIC than SPS and more suppression at mid rapidity than at forward rapidity [7, 8]. Both trends are contradicted by our data. Additionally, the J/ψ mean square transverse momentum, restricted to $p_T \leq 5$ GeV/c, shows little dependence on centrality. Various models of J/ψ production and suppression, which predict very different transverse momentum and rapidity dependencies, can be significantly constrained by the data presented here and recent results on open charm [11].

We thank the staff of the Collider-Accelerator and Physics Departments at BNL for their vital contributions. We acknowledge support from the Department of Energy and NSF (U.S.A.), MEXT and JSPS (Japan), CNPq and FAPESP (Brazil), NSFC (China), MSMT (Czech Republic), IN2P3/CNRS, and CEA (France), BMBF, DAAD, and AvH (Germany), OTKA (Hungary), DAE (India), ISF (Israel), KRF and KOSEF (Korea), MES, RAS, and FAAE (Russia), VR and KAW (Swe-

den), U.S. CRDF for the FSU, US-Hungarian NSF-OTKA-MTA, and US-Israel BSF.

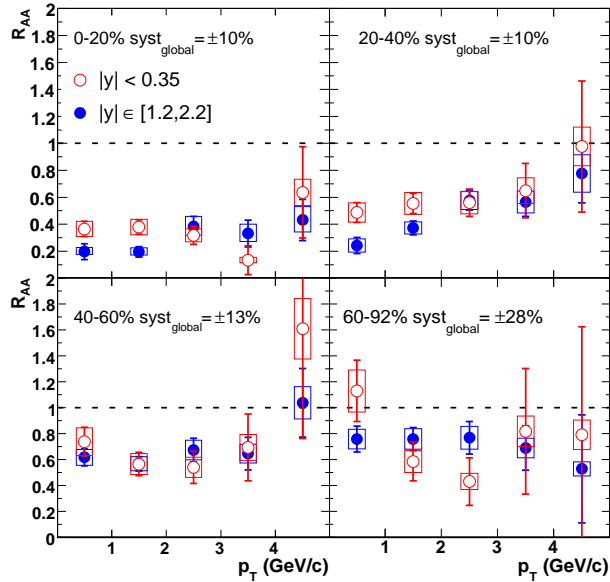


FIG. 3: J/ψ R_{AA} vs. p_T for several centrality bins in Au + Au collisions. Mid (forward) rapidity data are shown with open (filled) circles. See text for description of the errors.

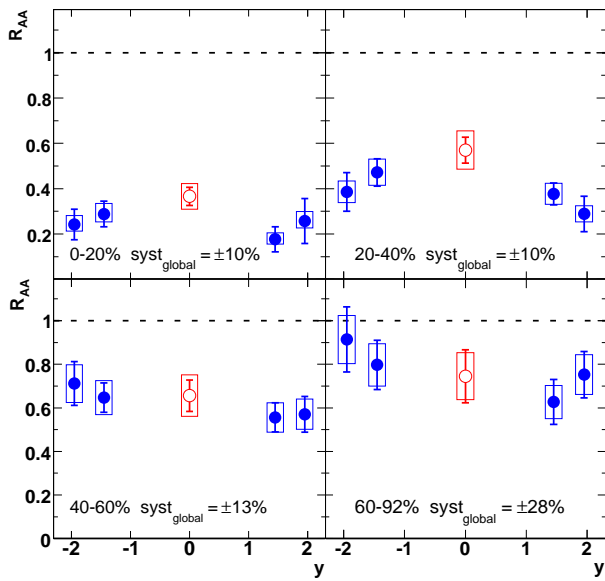


FIG. 4: J/ψ R_{AA} vs. y for different centrality bins. Open (filled) circles are for mid (forward) rapidity. See text for description of the errors.

* Deceased

† PHENIX Spokesperson: zajc@nevis.columbia.edu

- [1] F. Karsch, Lect. Notes Phys. **583**, 209 (2002).
- [2] T. Matsui and H. Satz, Phys. Lett. **B178**, 416 (1986).
- [3] F. Karsch et al., Nucl. Phys. **A715**, 701 (2003).
- [4] M. Asakawa and T. Hatsuda, Phys. Rev. Lett. **92**, 012001 (2004).
- [5] M. C. Abreu et al., Phys. Lett. **B410**, 337 (1997).
- [6] B. Alessandro et al., Eur. Phys. J. **C39**, 335 (2005).
- [7] Grandchamp et al., Phys. Rev. Lett. **92**, 212301 (2004).
- [8] Capella et al., Eur. Phys. J. **C42**, 419 (2005).
- [9] R. L. Thews and M. L. Mangano, Phys. Rev. **C73**, 014904 (2006).
- [10] S. S. Adler et al., Phys. Rev. Lett. **96**, 032301 (2006).
- [11] A. Adare et al. (2006), hep-ex/0609010.
- [12] S. S. Adler et al., Phys. Rev. Lett. **96**, 012304 (2006).
- [13] R. Vogt (2005), nucl-th/0507027.
- [14] A. Adare et al., Phys. Rev. Lett. **XX**, XXXXXX (2007).
- [15] K. Adcox et al., Nucl. Instrum. Meth. **A499**, 469 (2003).
- [16] S. S. Adler et al., Phys. Rev. Lett. **91**, 072301 (2003).

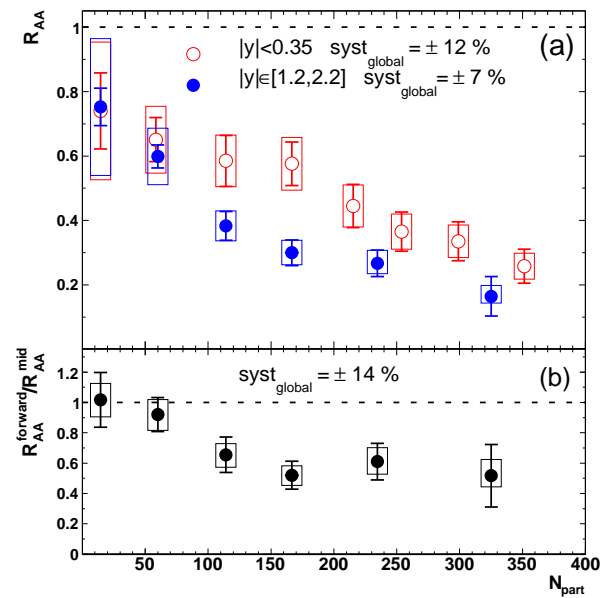


FIG. 5: (a) J/ψ R_{AA} vs. N_{part} for Au + Au collisions. Mid (forward) rapidity data are shown with open (filled) circles. (b) Ratio of forward/mid rapidity J/ψ R_{AA} vs. N_{part} . For the two most central bins, mid rapidity points have been combined to form the ratio with the forward rapidity points. See text for description of the errors.